Evidence and modeling of turbulence bifurcation in L-mode confinement transitions on Alcator C-Mod

As Published: 10.1063/1.5144444

Publisher: AIP Publishing

Persistent URL: https://hdl.handle.net/1721.1/136126

Version: Final published version: final published article, as it appeared in a journal, conference proceedings, or other formally published context

Physics of Plasmas ARTICLE scitation.org/journal/php

Evidence and modeling of turbulence bifurcation in L-mode confinement transitions on Alcator C-Mod

Cite as: Phys. Plasmas **27**, 052303 (2020); doi: 10.1063/1.5144444
Submitted: 2 January 2020 · Accepted: 15 April 2020 ·
Published Online: 14 May 2020

N. M. Cao,[1,a),b)] J. E. Rice,[1] P. H. Diamond,[2] A. E. White,[1] M. A. Chilenski,[1] P. C. Ennever,[1] J. W. Hughes,[1] J. Irby,[1] M. L. Reinke,[3] P. Rodriguez-Fernandez,[1] and Alcator C-Mod Team[1,c)]

AFFILIATIONS

[1]Massachusetts Institute of Technology, Cambridge, Massachusetts 02139, USA
[2]University of California San Diego, San Diego, California 92093, USA
[3]Oak Ridge National Laboratory, Oak Ridge, Tennessee 37831, USA

Note: This paper is part of the Special Collection: Papers from the 61st Annual Meeting of the APS Division of Plasma Physics.
Note: Paper TI2 3, Bull. Am. Phys. Soc. 64 (2019).
[a)]Invited speaker.
[b)]**Author to whom correspondence should be addressed:** normandy@mit.edu
[c)]See the author list of "Alcator C-Mod: research in support of ITER and steps beyond" by E.S. Marmar *et al.* 2015 Nucl. Fusion **55**, 104020.

ABSTRACT

Analysis and modeling of rotation reversal hysteresis experiments show that a single turbulent bifurcation is responsible for the Linear to Saturated Ohmic Confinement (LOC/SOC) transition and concomitant intrinsic rotation reversal on Alcator C-Mod. Plasmas on either side of the reversal exhibit different toroidal rotation profiles and therefore different turbulence characteristics despite the profiles of density and temperature, which are indistinguishable within measurement uncertainty. Elements of this bifurcation are also shown to persist for auxiliary heated L-modes. The deactivation of subdominant (in the linear growth rate and contribution to heat transport) ion temperature gradient and trapped electron mode instabilities is identified as the only possible change in turbulence within a reduced quasilinear transport model across the reversal, which is consistent with the measured profiles and inferred heat and particle fluxes. Experimental constraints on a possible change from strong to weak turbulence, outside the description of the quasilinear model, are also discussed. These results indicate an explanation for the LOC/SOC transition that provides a mechanism for the hysteresis through the dynamics of subdominant modes and changes in their relative populations and does not involve a change in the most linearly unstable ion-scale drift-wave instability.

I. INTRODUCTION

Confined plasmas are active, turbulent nonlinear systems, which demonstrate a complex dependency between external actuation and the plasma response. Of prime importance to magnetically confined fusion plasmas is the energy confinement time, the ratio of the plasma stored energy (the plasma response) to the applied heating power (the external actuation), which demonstrates a dependency on plasma parameters that cannot be described with a single scaling law.[1,2] Thus, to understand the behavior of fusion plasmas, it is necessary to understand the dynamics, which govern the plasma response, many of which are internal to the plasma, and how they could lead to different regimes of plasma behavior.

This work focuses on two transitions observed universally in tokamak plasmas: the Linear to Saturated Ohmic Confinement (LOC/SOC) transition and the intrinsic rotation reversal. The LOC/SOC transition refers to a break in the slope of the scaling of energy confinement with respect to density in Ohmic L-mode plasmas. There has been extensive experimental work characterizing the confinement transition and its link to L-mode density scaling.[3] The intrinsic rotation reversal refers to a spontaneous reorganization of the plasma

rotation in the absence of external momentum input. Typically, the rotation profiles transition from mostly flat co-current rotation profiles to hollow countercurrent rotation profiles. In response to ramps of plasma density, these two transitions are found to occur at the same critical density, the reason for which is unknown. This critical density is seen to correlate with a critical collisionality $\nu_* = (\nu_{ee}/\epsilon)/\omega_{be}$, where ω_{be} is the bounce time of electron banana orbits caused by trapping in the magnetic well and ν_{ee}/ϵ corresponds to the rate of electron detrapping due to collisions. There is also a wealth of other phenomenology associated with the transitions, including density profile peaking, non-diffusive cold pulse propagation, fluctuation spectrum changes, and impurity density asymmetries.[4–6] The concurrence of these two transitions suggests a link between the heat, particle, and momentum transport channels in tokamak core plasmas, reminiscent of how heat-flux driven turbulent Reynolds stresses are thought to trigger the L–H transition and lead to shear layer formation.

While there has been success in modeling the LOC/SOC transition *in silico*,[7–9] a self-contained physical picture of how changes in turbulence lead to the concurrence of these transitions and explain its observed properties remains elusive. Since drift wave turbulence is responsible for most of the heat, particle, and momentum transport in tokamaks, it has been conjectured that a transition from trapped electron mode (TEM) to ion temperature gradient (ITG) mode dominated turbulence could unify the confinement transition and rotation reversal. Experiments find changes in turbulent fluctuations across the LOC/SOC transition,[5,6,10,11] and modeling suggests that transport gradually changes from TEM-driven to ITG-driven across density ramps, which transition from LOC to SOC. However, studies find no clear change in the dominant ion-scale linear instability from TEM to ITG (either in the linear growth rate or driven quasilinear heat flux) at the transition itself.[8,12–15] Additional insights are needed to elucidate if and how a TEM/ITG transition is involved in the rotation reversal.

Here, we provide evidence that the two transitions are linked to a single nonlinear bifurcation of the plasma state in Alcator C-Mod, advancing the notion that LOC and SOC are representative of different states of nonlinearly saturated turbulence. We also show how elements of the bifurcation persist in auxiliary heated plasmas, suggesting its importance for understanding L-mode scaling in more generality. Additionally, we propose to identify the bifurcation as a partial turbulence population collapse, which involves the deactivation of a subdominant instability, providing a candidate theory for the reversal. This draws analogy with predator-prey models for the L–H transition, except in this case, not all ion-scale turbulent instabilities are quenched. Identifying the deactivated subdominant instabilities with an intermediate scale (between electron and ion scales), TEM provides a hypothesis for reconciling the lack of a clear transition in the linear behavior of TEM/ITG with the observed sharpness of the LOC/SOC and rotation reversal transitions.

First, the existence of a bifurcation is established through a set of experiments, which use hysteresis as a probe of the LOC/SOC transition and intrinsic rotation reversal. Hysteresis is the dependence of a system's state on its history and could result from memory or the evolution of hidden variables not tracked in the state space. This hysteresis is manifested as a bistability in the plasma response, corresponding to a range of experimental control parameters, which exhibit either LOC-like or SOC-like rotation depending on whether the plasma entered this range from an LOC-like state or a SOC-like state. Hysteresis in L-mode intrinsic rotation has been reported previously in multiple experiments.[10,11,16] The experiments presented expand upon results reported previously on Alcator C-Mod[15] and demonstrate nearly exact matches of mean plasma density and temperature, leading to different rotation and turbulent states in the same discharge in different plasma conditions. These show that changes in the mean drive profiles of density and temperature alone cannot be responsible for the LOC/SOC transition and rotation reversal. A quasilinear estimate of the turbulent fluxes, grouping related modes into families, enables the use of experimentally inferred fluxes to constrain possible changes in turbulence consistent with the observed transport. This analysis identifies the aforementioned partial turbulence collapse as a possible culprit for the nonlinear bifurcation, or alternatively that the quasilinear estimate for turbulent flux fails, also implying a change in the nonlinear state of the plasma.

The rest of this paper is organized as follows: Sec. II briefly reviews the literature surrounding TEM/ITG in LOC/SOC and rotation reversals and substantiates the assumptions made later on in the work. Section III presents the hysteresis experiments and the observed experimental characteristics. Section IV presents linear and quasilinear gyrokinetic analysis of the LOC/SOC transition and covers the impact on transport. Section V examines the constraints provided by the experiments on possible physical mechanisms underlying the observed bifurcation and whether or not they support the presented quasilinear analysis. We then conclude and discuss open questions and paths forward for further inquiry.

II. ROLE OF TEM/ITG IN LOC/SOC AND ROTATION REVERSAL

The conventional argument for why LOC/SOC is observed as the density increases is as follows: Ohmic heating primarily deposits power into the electrons. At low collisionality, the ions and electrons are only weakly thermally coupled, and TEMs are particularly virulent, leading to poor confinement. As the density increases, the collisionality serves both to improve the coupling of ions and electrons and to decrease the growth rate of TEMs through collisional detrapping of electrons. Main ion dilution $1 - (n_D/n_e)$ also tends to decrease, and T_e/T_i approaches 1 with increasing plasma density, leading to increased ITG growth rates. The TEM/ITG transition picture supposes that once the LOC/SOC transition density is reached, ITGs overtake TEMs as the key contributor to the confinement scaling. Since increasing collisionality does not have as large of an effect on the ITG drive, which tends to pin ion temperature gradients near marginal stability, the confinement scaling saturates. This argument appears to agree with reduced modeling of LOC/SOC using both analytic estimates of transport[7] and TGLF.[8,9] The roles of TEM and ITG instabilities are also implicated in producing the observed change in the core temperature response to edge cold pulses in perturbative laser blow off injection experiments in Ohmic plasmas,[17,18] where a gradual transition from TEM to ITG dominance correlates with the experimentally observed trend of transition from the core non-diffusive temperature inversion response to the core cooling response. Note, however, that historically, other mechanisms besides TEM stabilization have been proposed to capture the density scaling in LOC, such as turbulence at the skin depth scale,[19] which may play a role when electromagnetic effects are important.

The connection between drift wave mode and the rotation reversal is less clear. It is known that the profiles of intrinsic rotation observed in L-mode plasmas cannot be explained through purely diffusive and convective models and require some form of residual stress to explain. Here, the residual stress refers to the component of the momentum flux, which is proportional to neither the toroidal velocity nor its gradient. Generation of a net residual stress requires the breaking of a parity symmetry obeyed by the lowest order local gyrokinetics.[20–22] This is a broad and subtle topic, and the reader is directed to several recent reviews for an understanding of this topic.[23–25] Generally, it is expected that TEM and ITG should have different signs of residual stress due to the opposite sign of their group velocities. While simulations show a flip in rotation from TEM dominated plasmas to ITG dominated plasmas,[26,27] it is unclear how this connects to the experimentally observed rotation reversal. Recent simulations with global gyrokinetic codes have been able to reproduce the shape and magnitude of observed rotation profiles from experimental input profiles[28,29] and show both flat and hollow rotation profiles in plasmas, which are linearly ITG dominant.

The connection between linear stability and drift wave mode change is also subtle. It is generally difficult to precisely characterize the linear stability state of the plasma due to experimental uncertainty in the measured plasma profiles and gradients. Typically, when the rotation reversal occurs, it is found that ITG is the dominant linear instability at nominal gradient values in the radial locations where the toroidal rotation gradient changes. However, typically, variations of the driving gradients of 10–20% can lead to TEMs being the dominant linear instability, which are within $1–2\sigma$ of uncertainty around the inferred mean gradients. Experimentally, some changes in turbulent fluctuations have been observed when crossing the LOC/SOC boundary and the rotation reversal. On JET and Tore Supra, changes in reflectometry measurements, through synthetic diagnostics and nonlinear simulation, have been identified to correspond to the presence of a quasi-coherent TEM (QC-TEM) feature in LOC, which disappears upon transition into SOC.[30,31] It was noted in these studies that the QC-TEM feature depended not just on the presence of TEM but also on the saturated state of the turbulence. Changes in fluctuations have also been seen on Alcator C-Mod. Here, we will demonstrate how changes in turbulent fluctuation are seen at experimentally indistinguishable density and temperature profiles and that circumstantial evidence supports an interpretation of these changes reflecting changes in the underlying turbulence.

III. CHARACTERIZATION OF ROTATION REVERSAL HYSTERESIS ON ALCATOR C-MOD

The experiments presented here were run on Alcator C-Mod, a compact ($R = 0.67$ m, $a = 21$ cm), high-field (B_t up to 8.1 T) diverted tokamak with a molybdenum wall.[32] Two methods were used to realize the rotation reversal hysteresis: density control for Ohmic plasmas and ion cyclotron resonance frequency (ICRF) heating power modulation for auxiliary heated plasmas. The discharges were upper single null, with $B_t = 5.4$ T. The three experimental cases performed are shown in Table I. Case I has been reported in previous work.[15]

For all plasmas, line-average density control was achieved using edge fueling and a cryopump, along with the C-Mod two-color interferometer system for feedback control. For the Ohmic plasmas (cases I and II), the density modulations were triangle waves with amplitude

TABLE I. Experimental cases performed.

Case	I_p	Density modulation	ICRF modulation
I	0.8 MA	±10%	Off
II	1.1 MA	±10%	Off
III	0.8 MA	Constant	0.2–1.2 MW

±10% of a central value and a period much longer than the energy confinement time, 600 ms $\gg \tau_e \approx 25$ ms. Note that the impurity confinement time is of similar magnitude,[4] $\tau_I \sim \tau_e$. For the auxiliary heated plasma (case III), the ICRF heating modulation was also a triangle wave with the same period from 0.2 to 1.2 MW, with the intention of controlling the collisionality through changes in the electron temperature. For comparison, the Ohmic power was estimated to be 0.95 MW for a plasma at the same current in case I. Rotation profiles during the reversal evolved on timescales $\approx 4\tau_e$, slower than the modulation period. There was no beam injection in these plasmas, so the only particle source is at the edge. Additionally, on some discharges, a perturbed laser blow-off injection of CaF_2 impurity was performed to assess the robustness of the hysteresis to perturbation. Time traces from a representative case I discharge are shown in Fig. 1, where time points with matching line-integrated densities, but differing toroidal rotation, have been marked.

The coexistence of multiple rotation states at a given density can be visualized by plotting the line-average density vs the line-average toroidal velocity of the discharge as a hysteresis curve, as is done in Fig. 2. The plotted trajectories overlay closely, showing the robustness of the hysteresis phenomenon to noise and perturbation from laser blow-off (LBO) injection. Since the edge rotation is similar for the two rotation states, the change in the core rotation profiles indicates a change in the turbulently generated residual stress, implying that some aspects of the turbulence, yet to be determined, changes between the two states. This shows there exist two distinct states of turbulence, one exhibiting co-current rotation and the other countercurrent rotation, which can stably exist in this range of plasma density. As the density is slowly changed, the co-current rotation states continuously evolve to lower-collisionality LOC states, which corresponds to the "LOC-like" branch, while the countercurrent states continuously evolve to higher-collisionality SOC states, which correspond to the "SOC-like" branch. The rotation states between the two branches are transient and do not correspond to steady states of the plasma. The transition densities were found to match those from density ramp experiments, independent of the ramp rate. Thus, it makes sense to associate plasmas that exhibit co-current rotation with LOC-like turbulence and plasmas that exhibit countercurrent rotation with SOC-like turbulence. In addition, a hysteresis cycle in core electron temperature vs core line-average toroidal velocity is also plotted for case III, which demonstrates that the hysteresis in toroidal rotation persists for auxiliary heated L-mode plasmas, where the hysteresis is affected by ICRF heating modulation rather than by density modulation.

Kinetic profiles matched across the reversal for all three cases are shown in Fig. 3. The electron density was measured with the core and edge Thomson scattering system, while the electron temperature was measured with both the Thomson scattering system and the GPC-ECE system. Due to a diagnostic issue, local profiles of ion temperature and rotation were unavailable for these shots, so line-integrated data

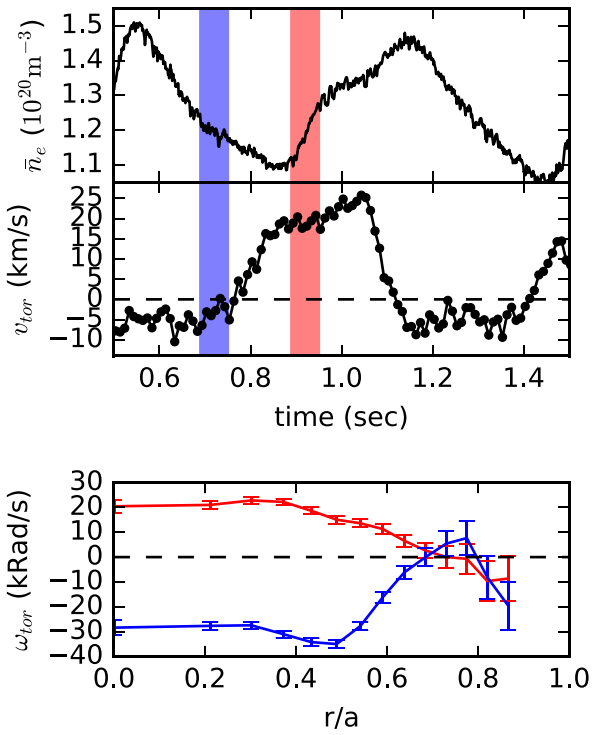

FIG. 1. Time trace of a 1.1 MA Ohmic discharge from the hysteresis experiments (top) and representative toroidal rotation profiles from another discharge at the same current (bottom). The two times marked by the blue and red bars have nearly the same line-average density, electron and ion temperatures, but different core toroidal velocities. The rotation profiles are similar at the edge but diverge in the core. The region where the rotation diverges and the shear is non-zero will be referred to as the rotation reversal region.

inferred using Bayesian techniques[33] are shown instead. Additionally, local ion profiles from previously published discharges in Rice *et al.*,[4] whose experimental parameters were replicated in this set of experiments, are shown when available. The fits displayed use data time-averaged over 60 ms and utilize Gaussian Process Regression to provide rigorous estimates of the error bars on the profiles and their gradients.[34] These error estimates take into account the statistical and systematic uncertainties of the data, given by error bars on individual measurements and systematic uncertainties due to the unknown form of the fit, provided by a prior on the hyperparameters of the fit. The latter can have a large effect on the error bars, so their effect is properly taken into account by sampling the hyperparameter space using Markov Chain Monte Carlo. As in Chilenski *et al.*,[34] a non-stationary squared exponential kernel with a tanh length scale shape is used. Note that the priors differ from those used for the previously reported profiles, as they were changed to better capture the flattening effect of sawteeth inside the sawtooth mixing radius. For all three cases, the profiles and gradients responsible for determining the linear stability characteristics of the drift-wave turbulence overlay each other very closely. This confirms previous analysis that drift-wave stability is not responsible for the reversal.

Despite the nearly identical kinetic profiles, differences in fluctuations can be observed in the 1.1 MA Ohmic and 0.8 MA RF-heated cases. Data are presented here from the Phase Contrast Imaging (PCI) system on C-Mod, which is sensitive to line-integrated density fluctuations with wavevector components in the major radial direction of $k_R < 30\,\mathrm{cm}^{-1}$, corresponding to $k_R\rho_s \lesssim 2.5$. In these cases, the PCI picks up high-frequency "wing" features in the LOC case, as has been previously reported.[10,11,35,36] This is shown by the PCI spectra in Fig. 4 and demonstrates that measured fluctuation spectra can change even at matched conditions. One of the characteristic features observed about these PCI wings is an asymmetry in the $\pm k_R$ spectrum. The time evolution of a metric capturing this asymmetry is also plotted in Fig. 4. It is interesting to observe that for the 1.1 MA Ohmic case, there is an asymmetry in the time evolution of fluctuations for the forward and reverse transitions. Going from LOC to SOC, when the shear layer forms, the fluctuations evolve on a timescale faster than the rotation reversal. Conversely, going from SOC to LOC, when the shear layer collapses, the fluctuations evolve on a timescale similar to the rotation reversal.

Since PCI measurements are line-integrated, interpreting changes in PCI spectra can be challenging. The PCI sight lines are vertical and intersect magnetic flux surfaces twice, once toward the top of the tokamak and once toward the bottom. The sign of the projection of k_θ onto k_R changes between these two intersections, so a $\pm k_R$ asymmetry is usually interpreted as an up-down fluctuation asymmetry. Note that k_R could be either larger or smaller than k_θ, depending on the angle of

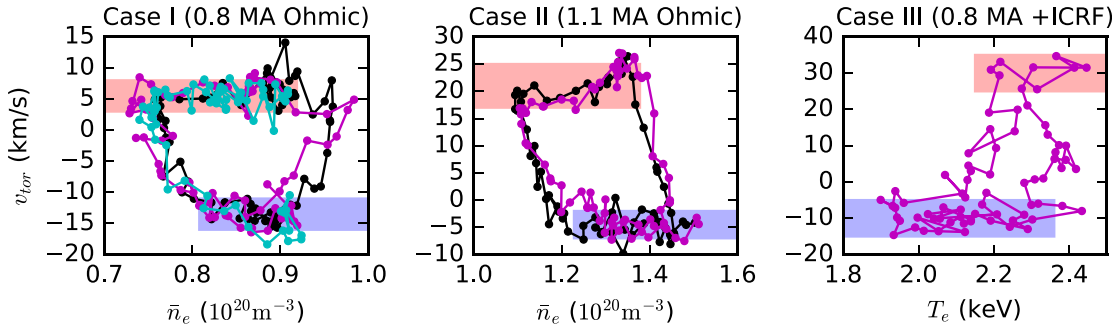

FIG. 2. Trajectories of several discharges as hysteresis plots for different experimental cases. Different colors in each plot correspond to different discharges. The discharges all demonstrate clearly separated rotation states at the same density for the Ohmic cases and core electron temperature for the ICRF heated case. These states have been highlighted in red and blue. Note that discharges in cyan and magenta were perturbed using laser blow-off injections. The discharge in the left frame plotted in cyan does not reach the required density to transition from the LOC-like branch to the SOC-like branch, so it does not complete a full hysteresis loop.

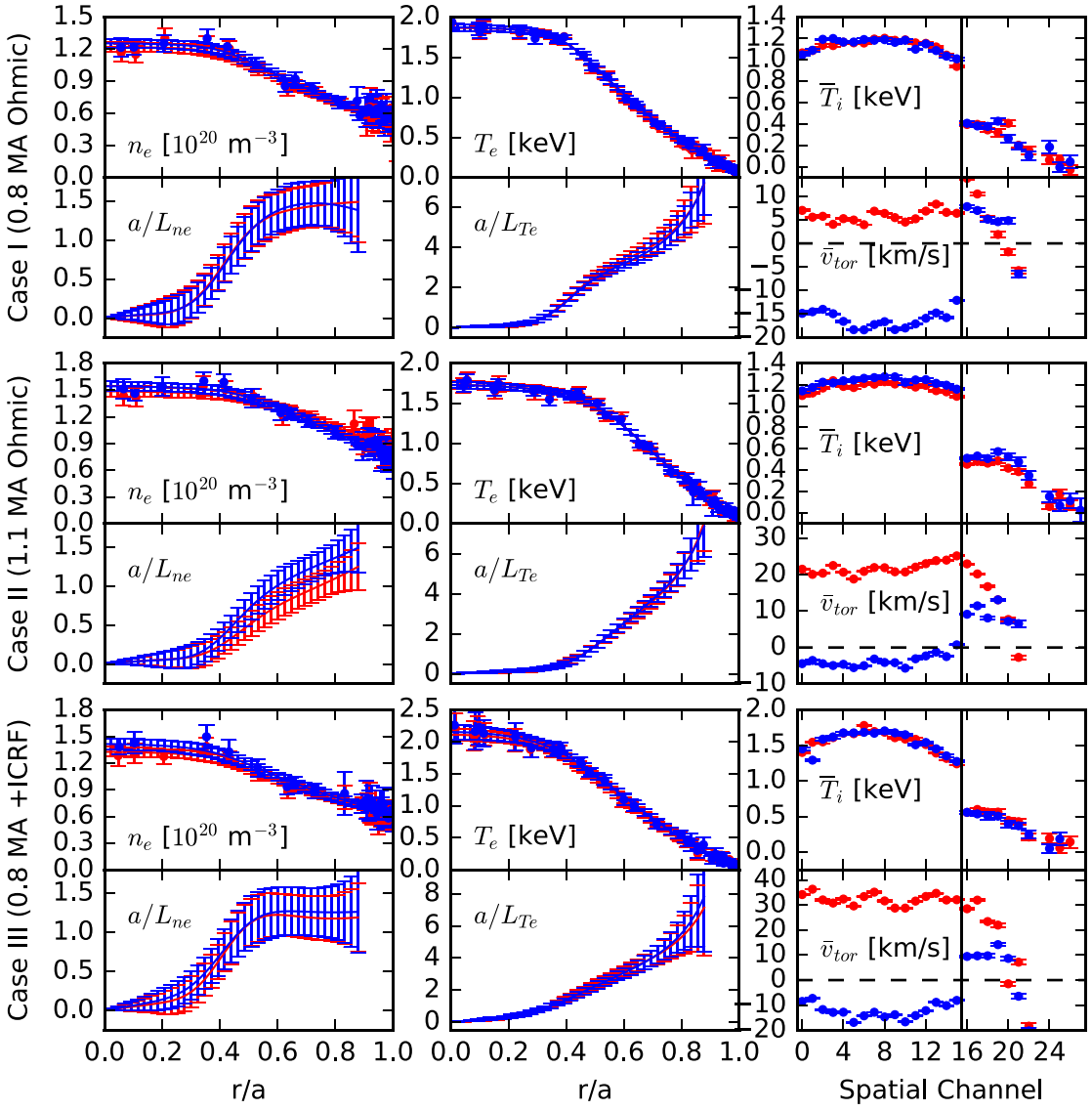

FIG. 3. Profiles and gradients of electron density (left column), temperature (center column), and line-integrated ion temperature and rotation (right column), for the three experimental cases. The co-current rotation LOC-like profiles are shown in red, and the countercurrent rotation SOC-like profiles are shown in blue. For the electron profiles, the raw data are shown by the scatter points, and the GPR fit is shown as a smooth profile. The timeslices were chosen to show profiles that overlay each other well within experimental uncertainty. For the ion measurements, different spatial channels provide coverage of different radial locations in the plasma. There is a discontinuity in plasma coverage at channel 16, which is demarcated by a solid black line.

incidence to the flux surface and the radial wavevector k_r. Although it is difficult to precisely localize the radial location of the measured fluctuations, previous work suggests that the wing features are not an edge fluctuation.[10] Furthermore, it was shown via a PCI masking technique[37] that the features propagate in the ion diamagnetic direction in the laboratory frame. This is consistent with the expectation that in LOC, the Doppler shift dominates the plasma frame frequency of the drift-wave modes and that the co-current rotation is in the ion diamagnetic direction in the low-field side where the drift-wave fluctuations originate. The roughly 700 kHz real frequency extent of the wings in the 1.1 MA Ohmic case corresponds to an angular frequency in the laboratory frame of $4.4c_s/a$ at $r/a = 0.6$. If this frequency were the result of an $E \times B$ Doppler shifted mode with zero real frequency in the plasma frame at $r/a = 0.6$, it would require the mode to have a toroidal mode number $n \approx 440$, although this estimate is crude due to uncertainty in the magnitude of the toroidal rotation and the radial location of the mode. Using $k_\theta \approx nq/r$, this would correspond to $k_\theta \rho_s \approx 3.7$. It would be difficult to observe ITG in the frequency range of the wings, which typically has $|\omega_r| \lesssim c_s/a$ and $k_y \rho_s \lesssim 1$. In contrast, TEMs with $k_\perp \rho_s \gtrsim 1$ and $|\omega_r| \gtrsim c_s/a$ may more plausibly be observed in the wing frequency range. Additionally, the weakly dispersive nature of the wings (i.e., fluctuations having nearly constant phase velocity) is

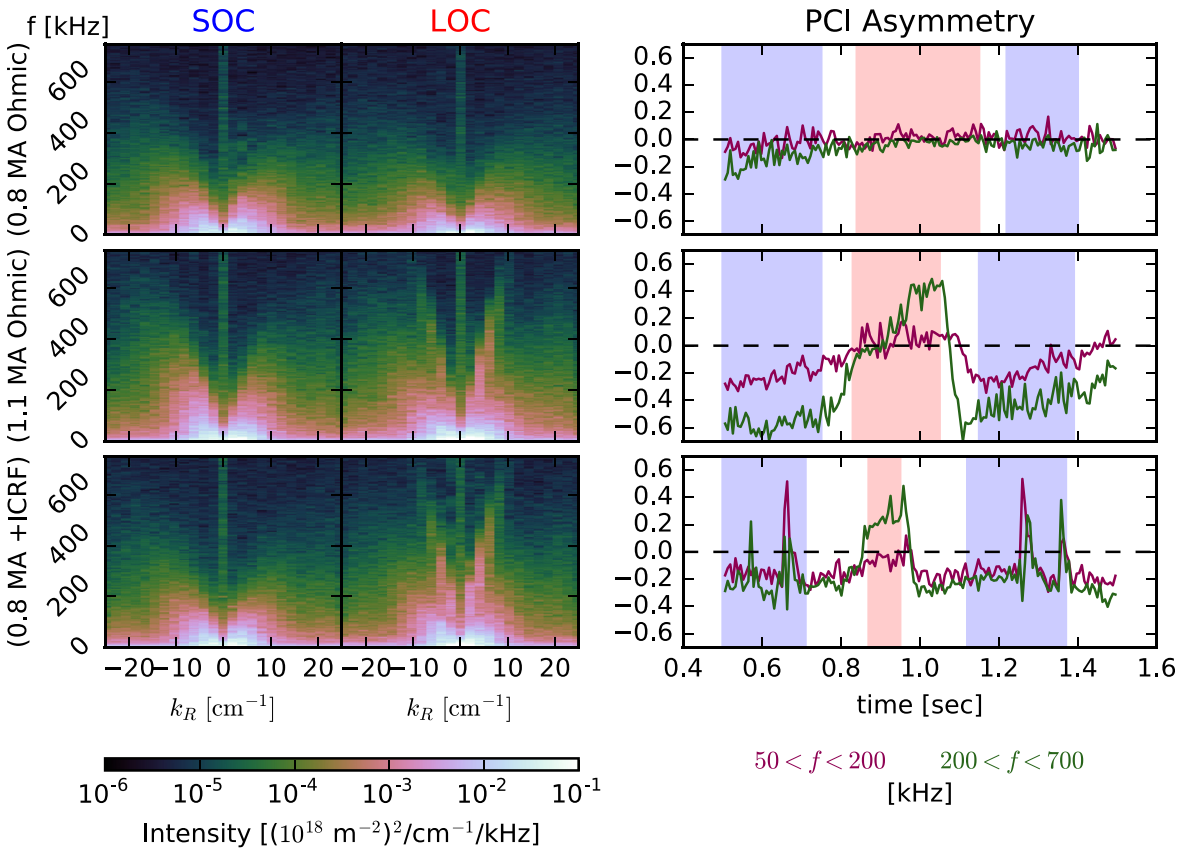

FIG. 4. Spectrograms $S(k_R, f)$ of PCI fluctuations for the three experimental cases corresponding to the profiles in Fig. 3 (left) and asymmetry $\frac{P_+ - P_-}{(P_+ + P_-)/2}$ for certain frequency bands plotted against time (right). While there is no discernible difference between the PCI spectra in the 0.8 MA Ohmic case, there are clear visible "wing" features in the 200–700 kHz range for the other two cases. The evolution of these features in time is visualized by the asymmetry in the $\pm k_R$ parts of the spectrum at the given frequency bands. Times corresponding to steady co- or countercurrent rotation are shaded in red and blue, respectively.

consistent with intermediate scale $k_\theta \rho_s \approx 2$–5 TEMs, as will be discussed in detail later. Note that the frequency response of the PCI detectors decays exponentially with frequency,[38] so the attenuation of the wings at high frequency does not necessarily represent the attenuation of fluctuations in the plasma at that frequency.

One possibility for the lack of visible wings in the 0.8 MA Ohmic LOC case is the weaker Doppler shift (roughly 2–4 times smaller) in that case compared to either the 1.1 MA Ohmic case or 0.8 MA ICRF heated case, which may be insufficient to bring the wings above the strong fluctuations below 200 kHz. The wings not being discernible from the low frequency fluctuations, in combination with a possible difference in the ratio of edge to core fluctuation levels, may explain why the asymmetry is much weaker or does not appear in the 0.8 MA Ohmic case. Note that the gyro-Bohm normalized anomalous fluxes are larger in the 1.1 MA Ohmic case than they are in the 0.8 MA Ohmic case.

IV. LINEAR AND QUASILINEAR GYROKINETIC MODELING

Linear and quasilinear gyrokinetic analysis of the case I 0.8 MA Ohmic plasma for the matched profiles was previously reported.[15] In that Letter, it was found that there was no change in dominant linear instability across the rotation reversal for the matched profiles. Furthermore, quasilinear analysis identified a subdominant mode transition at intermediate $k_y \rho_s \gtrsim 1$ consistent with the transport inferred for the matched profiles. Rather than focusing on matched profiles, the analysis presented here focuses on timeslices right before the LOC to SOC transition to try and characterize possible changes in turbulence as the transition occurs. Due to the lack of ion profile data from the presented experiments, linear and quasilinear gyrokinetic analysis was performed on density ramp shots from Rice *et al.*,[4] corresponding to case I and case II.

The gyrokinetic code CGYRO[39] was used in initial value mode, with gyrokinetic ions and electrons and one gyrokinetic impurity species to match Z_{eff}. The Sugama model collision operator was used with experimentally calculated collision rates, experimental geometry was used, and $\delta A_\parallel$ fluctuations were included. The calculated linear growth rates and real frequencies are plotted in Fig. 5. The results of the analysis confirm results that have been reported previously: near the transition, the dominant ion-scale instability is ITG. An interesting observation is that near the transition, the scales $k_y \rho_s$ where TEMs are dominantly unstable separate from the scales where ITGs are dominantly unstable, leaving a region near $k_y \rho_s \approx 1$ of modes, which are

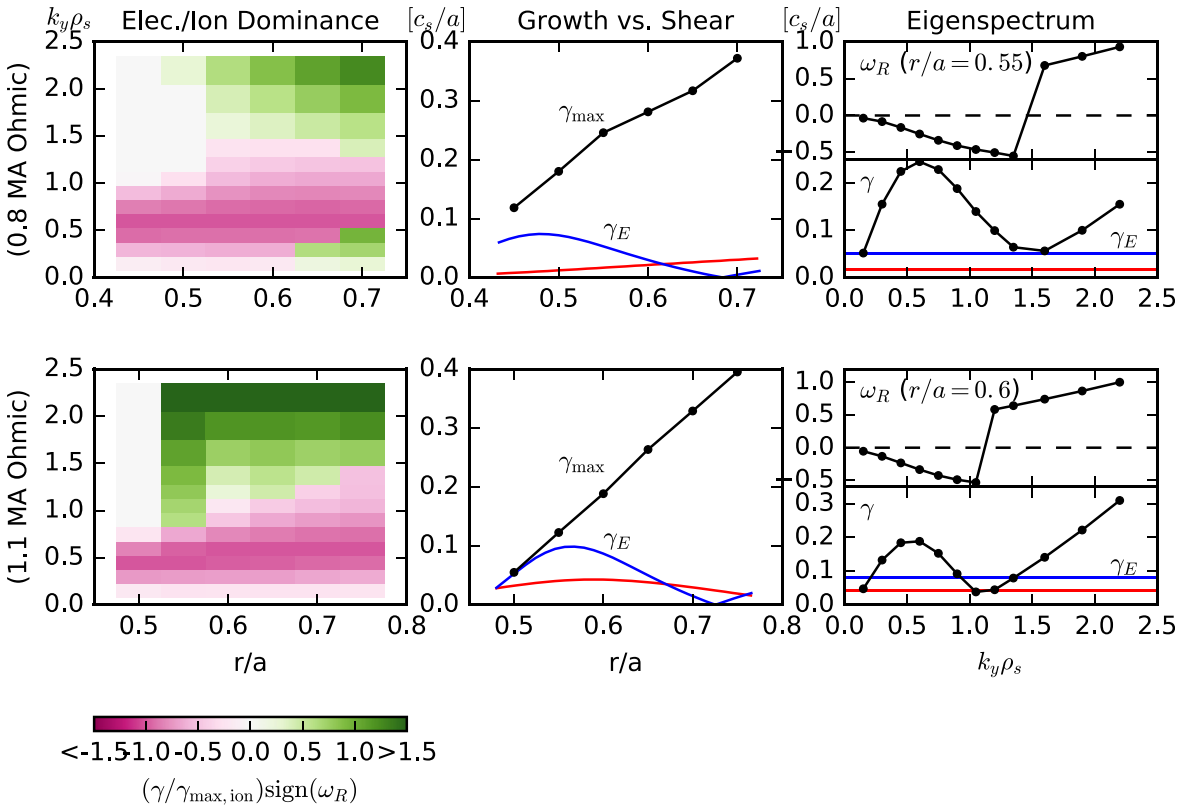

FIG. 5. Plot of dominant linear instability as a function of $k_y\rho_s$ and r/a (left), the maximum ion scale linear growth rate against $E \times B$ shear (center), and the real frequency and growth rate plotted for a single radial location in the reversal region, with $E \times B$ shear plotted for comparison (right). Case I (top row) and case II (bottom row) were analyzed. The negative frequency corresponds to ion-direction turbulence. For the dominant linear instability, the growth rates are normalized to the maximum ion scale linear growth rate and show that ion-direction turbulence remains dominant over the entire plasma radius shortly before the rotation reversal. Next, a plot of the maximum ion scale growth rate against the $E \times B$ shearing rate calculated from force balance is shown, where red and blue correspond to LOC and SOC, respectively. Note that the shearing rate reaches a significant fraction of the maximum ion scale growth rate. Finally, the linear spectrum for a single radius is shown.

strongly subdominant to the dominant ion-scale instability in the linear growth rate. Additionally, a plot of the largest ion-scale growth rate is plotted against the $E \times B$ shearing rate calculated from force balance for co- and countercurrent rotation profiles in Fig. 5.

To better understand the impact of the modes on transport and diagnose the turbulent state of the plasma, we adopt a quasilinear transport approximation (QLTA). This is the model used in the previous analysis[15] and will be reintroduced here. In this QLTA, the turbulent fluxes (e.g., the electron heat flux Q_e) are expressed as the sum of a quasilinear mode weight (for electron heat flux, this will be denoted $W_{Qe,k}$) times an averaged mode intensity (also called the spectral weight; in this case, $\langle\bar{\phi}_k^2\rangle$) for each linear eigenmode indexed by wavenumber k. For example, writing this explicitly for the electron heat flux,

$$Q_e = \sum_k W_{Qe,k}\langle\bar{\phi}_k^2\rangle. \tag{1}$$

Adopting this model allows the separation of the linear physics of the plasma, encoded into the quasilinear weights here assumed to be determined entirely by the structure of the linear eigenmodes, from the nonlinear physics of the plasma, encoded into the mode intensities determined by the nonlinear turbulence saturation mechanisms active in the plasma. While the validity of this approximation has not been rigorously established, in practice, mQLTA has been surprisingly successful. Quasilinear weights have been found to match weights calculated from fully nonlinear simulation.[40] Density-temperature fluctuation cross-phases, which are related to the quasilinear weights, have been observed to match experimental measurements.[41,42] This model also underlies modern quasilinear transport codes such as TGLF[43] and QualiKiz,[44] which have shown success in replicating heat and particle transport in LOC/SOC transition scans.

Here, instead of being used in a predictive fashion, mQLTA is used in a diagnostic fashion. Using power balance, experimentally derived turbulent fluxes can be utilized to provide a constraint on the possible mode intensities. Three fluxes are used: the electron and ion heat fluxes and the electron particle flux. This analysis uses the power balance code TRANSP[45] and subtracts out the neoclassical component of the fluxes calculated from the code NEO.[46] The resulting anomalous fluxes are plotted in Fig. 6. If the spectrum is discretized into N modes, then Eq. (1) and the corresponding equations for the other fluxes can be viewed as a $3 \times N$ matrix equation, as in the following equation:

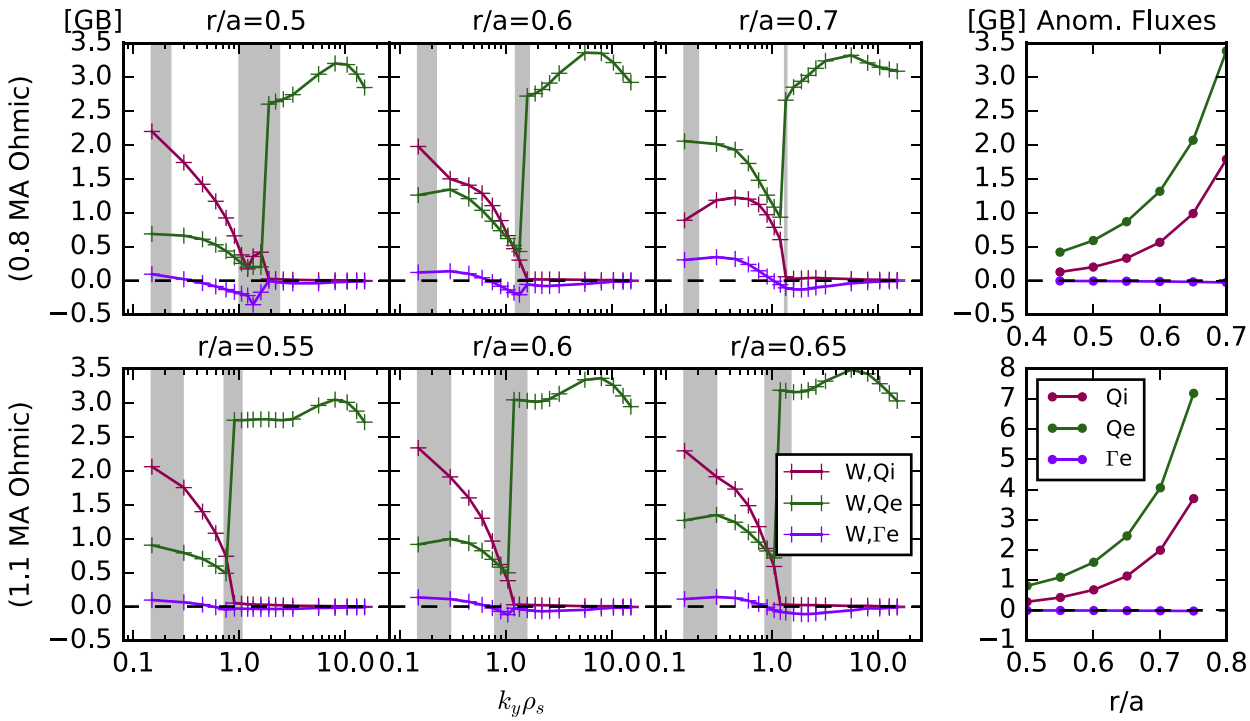

FIG. 6. (Left) The quasilinear weights are shown for the most unstable drift wave modes at different radial locations, shortly before the rotation reversal, for the two Ohmic cases. (Right) The anomalous fluxes inferred for this time slice are shown, plotted as a function of the radius. Both the quasilinear weights and anomalous fluxes are plotted in gyro-Bohm units. The plot of anomalous fluxes shows how the particle flux is nearly zero, when compared to the ion and electron heat fluxes in gyro-Bohm units. For the quasilinear weights, the regions marked in gray are the "subdominant" regions, where $\gamma_k < 0.4\gamma_{max}$ for case I and $\gamma_k < 0.7\gamma_{max}$ for case II. These gray regions define the subdominant mode families used in the quasilinear analysis.

$$\begin{bmatrix} Q_i \\ Q_e \\ \Gamma_e \end{bmatrix} = \begin{bmatrix} W_{Qi,k_1} & W_{Qi,k_2} & \dots \\ W_{Qe,k_1} & W_{Qe,k_2} & \dots \\ W_{\Gamma e,k_1} & W_{\Gamma e,k_2} & \dots \end{bmatrix} \begin{bmatrix} \langle \bar{\phi}^2_{k_1} \rangle \\ \langle \bar{\phi}^2_{k_2} \rangle \\ \vdots \end{bmatrix}$$
$$\approx \begin{bmatrix} W_{Qi,I} & W_{Qi,II} & \dots \\ W_{Qe,I} & W_{Qe,II} & \dots \\ W_{\Gamma e,I} & W_{\Gamma e,II} & \dots \end{bmatrix} \begin{bmatrix} \langle \bar{\phi}^2_I \rangle \Delta k_I \\ \langle \bar{\phi}^2_{II} \rangle \Delta k_{II} \\ \vdots \end{bmatrix}. \quad (2)$$

In the full system, N will be very large or infinite, so a naive application of the flux constraint leaves the mode intensities highly underdetermined. However, for the purpose of broadly determining trends in transport of the plasma, we do not need the detailed shape of the mode spectrum. For example, at electron scales corresponding to $k_y\rho_e \lesssim 1$, electron temperature gradient (ETG) modes will exhaust primarily electron heat flux without exhausting ion heat or particle flux since ions will behave adiabatically at that scale. Thus, the net effect of ETGs on the turbulent fluxes can be well approximated using only one degree of freedom, instead of using one degree of freedom per mode. This motivates the construction of a reduced transport model where similar modes are lumped together into "families." To calculate the total turbulent fluxes, the sum over modes is replaced with a sum over families, using quasilinear weights and spectral weights averaged over the modes in the family. Additionally, here an explicit spectral width Δk has been included, which captures the number of modes in the original sum that the family replaces. This is represented in matrix form as in the second line of equation (2), where the families are enumerated by Roman numerals I, II, III,… Note that the product $\langle \bar{\phi}^2_I \rangle \Delta k_I$ represents a family integrated spectral weight, while $\langle \bar{\phi}^2_I \rangle$ alone is the family averaged spectral weight.

Previously, this reduced family model was applied to the matched profile cases to identify a candidate subdominant mode transition, where the deactivation of an intermediate scale $k_y\rho_s \gtrsim 1$ instability was found to be consistent with the observed transport. Here, a refinement of that analysis is presented. Several radial locations were chosen for analysis, starting with the location of maximum and proceeding radially outward until the points were outside the rotation reversal region. The quasilinear weights calculated from CGYRO are shown in Fig. 6, for case I and case II. Despite being at different currents, the quasilinear weights look very similar between the two cases, with key features that are present in all analyzed locations:

- At ion scales $k_y\rho_s \lesssim 1$, the modes primarily exhaust ion heat flux, although there is a significant electron heat flux component as well. These modes are also thought to be responsible for most of the momentum transport in the plasma, as momentum will primarily be carried by ions. The electron particle transport starts outward at low k but becomes increasingly inward directed as higher k values are approached. For locations within the rotation reversal region, this inward trend is strong enough to reverse the

direction of the particle flux. This ITG particle flux trend can be understood through a kinetic picture.[47] Collisions and diffusion cause outward particle fluxes, as is the case at low k. Ion finite Larmor radius effects push the phase velocity of higher k modes closer to zero, causing the modes to be resonant with lower energy particles. Since temperature gradients produce an energy dependence in the radial gradient of the background Maxwellian distribution function, which is of opposite sign to that produced by a density gradient at low energies, modes that are resonant with lower energy particles produce a stronger inward thermally driven particle flux. These changes manifest as a change in the phase relation between density and potential fluctuations, leading to different quasilinear weights.

- At intermediate scales $k_y\rho_s \sim 1$, both ITG and a combined TEM/ETG branch are present. Occasionally, ubiquitous modes[48] (modes with real frequency $\approx$0) can be observed in linear simulations at this scale. ITG and ubiquitous modes present at this scale tend to have strongly inward particle flux. TEMs that are active at this scale also have inward particle fluxes.
- At electron scales $k_y\rho_s \gg 1$, only a combined TEM/ETG branch is present. These modes are characterized by nearly adiabatic ions due to ion gyroaveraging over the small scales and hence have weak ion heat and momentum flux and weak particle flux due to the ambipolar nature of transport in axisymmetric systems.[49]

Additionally, it was found that electromagnetic perturbations contributed <5% to the quasilinear weights, so the transport is dominantly driven by electrostatic turbulence. Note that these weights were not found to be nearly identical between the matched LOC and SOC states in previous work.[15]

Proceeding with the identification of families using the quasilinear weights, here we classify modes into dominant or subdominant families by the following criterion: At the location of maximum $\omega'_{tor}(r)$, calculate the ratio $\alpha \equiv \gamma_E/\gamma_{\max}$. γ_{max} is the maximum ion scale linear growth rate, and $\gamma_E = \frac{r}{q}\frac{\partial\omega_0}{\partial r}$ is the shearing rate from ω_0, the $E\times B$ rotation rate calculated using force balance. Using the shearing rates right after the rotation reversal results in an α value of about 0.4 for the 0.8 MA Ohmic case I and about 0.7 for the 1.1 MA Ohmic case II. Then, across the entire profile, the subdominant modes are defined as modes with $\gamma_k < \alpha\gamma_{\max}$, where γ_k is the maximum growth rate at each k_y. At the location of maximum shear, the subdominant modes correspond to modes, which, a naive application of the "Waltz rule"[50] would suggest, are quenched by the mean $E\times B$ shear in SOC, although the derived constraints are independent of whether or not the modes are actually quenched by the flow shear. Each contiguous component of subdominant modes on each branch of dispersion is grouped into a single family, allowing the identification of six families, shown in Table II, with their main properties summarized. The naming scheme is somewhat arbitrary, as, for example, there is no discrete delineation between TEM and ETG. Additionally, note that this classification based on the linear growth rate is not the only possible way to group the modes into families, and consideration of other mechanisms including nonlinear mode coupling may suggest different classifications.

With these families identified, the additional constraint that mode intensities must be non-negative distinguishes two qualitatively different solutions consistent with the transport constraints imposed by Eq. (2), based on whether or not the subdominant modes are active. Since neutral penetration from the edge is low and there is no beam fueling on Alcator C-Mod, the particle flux in the core is nearly zero. The neoclassical particle flux is not large enough to balance a significant turbulent particle flux, so the active modes must have a roughly balanced net particle flux. So, one possible solution is that in the rotation reversal region, only the dominant modes ITGb and TEMb/ETG are active, and the subdominant modes are inactive. The particle flux constraint is satisfied primarily within the modes of ITGb, possibly with a small additional contribution from TEMb. This is possible because the particle flux weight of these modes averages to nearly zero for weights in the rotation reversal region. This leads to a narrower k spectrum of ion-scale turbulence, with electron direction turbulence quenched at ion-scales, corresponding to a SOC-like regime. Note that at large enough r/a, an increasingly large outward particle flux is driven by ITG due to increasing collisionality, so it is not possible for the particle balance constraint to be satisfied within ITGb alone. This necessitates significant activity from TEMa/b at these radii. Another possibility is to have both dominant and subdominant modes active. For the other solution, the subdominant ITGa is active, so either or both of ITGc and TEMa/b must have significant activity in order to balance the net particle flux. This leads to a broader k spectrum, with possibly intermixed ion- and electron-direction turbulence at ion-scales, corresponding to a LOC-like regime.

Since the SOC-like and LOC-like regimes continuously connect to the higher collisionality countercurrent rotation and lower

TABLE II. List of families used in the quasilinear analysis.

Family	Description
ITGa	Low-k subdominant ITG, which always has outward particle flux
ITGb	Mid-k ITG, which has nearly balanced particle flux inside the rotation reversal region
ITGc	High-k subdominant ITG, which has strong inward particle flux inside the rotation reversal region
TEMa	$k_y\rho_s \sim 1$ subdominant ∇T_e driven TEM, which always has inward particle flux. Ubiquitous modes are sometimes observed at this scale.
TEMb	$k_y r_b \lesssim 1$ ∇T_e driven TEM, where r_b is the typical banana orbit width. This also always exhibits inward particle flux, although it is particularly strong outside the rotation reversal region. Some metrics of subdominance, such as comparing $\gamma/k_\perp^2$, find all TEMs to be subdominant and so do not have a TEMb family.
ETG	$k_y r_b \gtrsim 1$ ETG, which exhausts primarily electron heat flux.

collisionality co-current rotation branches of the turbulent bifurcation, respectively, it is inferred that the rotation physics of ITG dominant or TEM dominant (but possibly ITG active) turbulence continues to be relevant closer to the transition in their respective regimes. The changes suggested by this model are illustrated schematically in Fig. 7 and their consequences summarized in Table III. One key implication is that despite heat transport being the principal externally driven means of turbulent free energy release in the plasma, modes that are subdominant in heat transport can play a role in determining the behavior of transport in other channels, such as particle or momentum transport.

V. PHYSICAL FEEDBACK MECHANISMS OF THE BIFURCATION

In order to fulfill the stated goal of understanding the feedback mechanisms leading to the LOC/SOC transition, we would like to know what constraints hysteresis places on the possible physical mechanisms underlying the observed dynamics. In the typical view of plasma turbulence, fluctuations grow due to down-gradient fluxes in the plasma, which release thermodynamic free energy. In a quasi-linear picture, the energy of these fluctuations is located mostly in linear eigenmodes of the system, and the total transport is determined when pumping of each mode by the linear growth rate for the relaxed mean profile balances energy transferred out of the mode by nonlinear interactions on average, leading to a saturated state of turbulence. This model was implicit in the earlier sections, particularly in the discussions of Sec. II. These assumed that a decrease in the linear growth rate of the turbulence would lead to a decrease in the saturation level of the turbulence and hence a reduction in transport. However, upon looking at this viewpoint critically, it leaves open the possibility that changing saturation mechanisms, rather than changing linear drives, could cause the transition. This section will describe some possibilities for changes in saturation, which could underlie the turbulent transition.

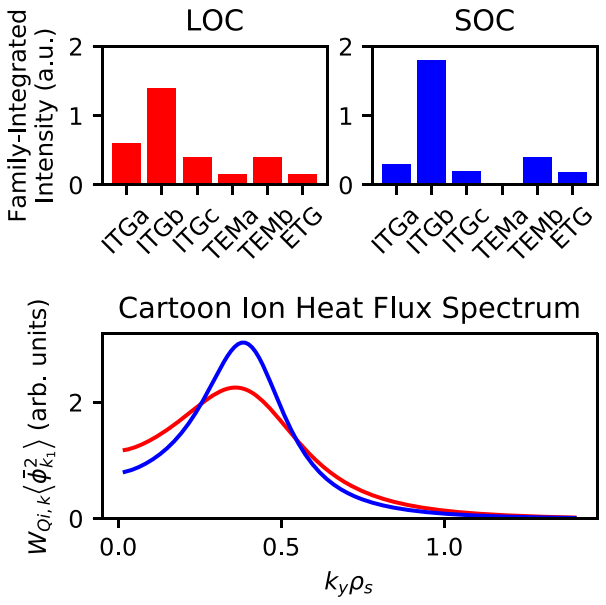

FIG. 7. A qualitative illustration of the proposed LOC/SOC transition. (Top) Example of six mode family integrated intensities, which would be consistent with the inferred transport via Eq. (2). Note that the exact ratios between families are underconstrained, so these are only illustrative solutions. In SOC, the subdominant families ITGa/c and TEMa are quenched in a way that respects particle flux constraint. (Bottom) An example ion heat flux spectrum, which is consistent with the above mode families. Note that the SOC spectrum in blue is narrower than the LOC spectrum in red.

TABLE III. Summary of the consequences of the two possible turbulent states predicted by mQLTA.

Turbulent state	LOC	SOC
Active mode families	Broad ITG Ion- and electron-scale TEM ETG	Narrow ITG Electron-scale TEM ETG
Particle flux balance	ITG balances TEM	Balance within mid-k ITG
Electron heat transport	Ion and electron scale	Primarily electron scale
Torque balance	TEM and ITG	ITG dominates

While this work does not suggest a mechanism leading to the observed bistability of the turbulent state, it does identify constraints on the possibilities. The experimentally observed matched density and temperature profiles, both in the mean value and gradients, show that the bistability cannot be explained by changes in the linear instability drive terms alone. Although not systematically ruled out, the robustness of the hysteresis to perturbation from LBO injection also suggests that the crossing of an undetected linear stability boundary is not responsible for the transition. This is due to the large effect of LBO on the linear stability of the plasma.[17,18] Additionally, while profile shear has been identified as being important to intrinsic rotation,[29,51] these experiments suggest that changing profile shear is not responsible for the transition itself. However, the experiments do not rule out profile shear being responsible for setting the final steady-state shape of the rotation profile.

Local mean-field mechanisms for bistability are not entirely ruled out by the profiles, as the change in the mean rotation profile could feedback on the plasma turbulence. The $E \times B$ flow shear is not large enough to entirely quench the ion-scale turbulence, but the shearing rate is a significant fraction of the maximum linear growth rate at ion-scales, as shown in Fig. 5. Thus, the flow shear could play a role in the saturation of subdominant modes, creating a situation resembling a "population collapse" posited by predator-prey models of turbulence at the L–H transition (see, e.g., Diamond *et al.*).[52] Here, only a portion of the ion scale spectrum collapses at the transition due to the formation of a shear layer, instead of its entirety. Experimentally, this could be manifested in several ways: for example, as a change in fluctuation intensity spectra, fluctuation correlation lengths, or fluctuation cross-phases, all of which can be measured on present-day devices. However, nonlinear mode interactions are important in determining the response of modes to the $E \times B$ flow shear.[50,53,54] Thus, it is premature to conclude that changing flow shear is the primary driver of changing turbulence on the basis of the comparison of the linear growth rate of subdominant modes to the shear rate.

Looking beyond mean field dependencies, other mechanisms for bistability could involve a change in meso- or micro-scale structures, leading to a change in the mode-mode or mode-zonal flow nonlinear energy transfer. At a basic level, ITGs are predominantly observed to saturate by coupling to zonal flows, while TEM saturation is found to be insensitive to the presence of zonal flows in some parameter regimes.[55–58] $T_e/T_i \approx 1.2-1.4$ and $\eta_e \approx 2-3$ in the rotation reversal region, which may be a regime of weak zonal flow damping of TEMs. Simulations have suggested the importance of turbulent particle transport or zonal density in the saturation of TEMs,[56,57] although it is unclear why zonal flows become an ineffective saturation mechanism and what relevance if any this plays in the LOC/SOC transition. The rest of this section will discuss some possibilities for changes in meso- or micro-scale structures relevant to the LOC/SOC transition, although the suggestions are not mutually exclusive and do not comprise an exhaustive list.

One such change is suggested by Fig. 8, where the perpendicular group velocity in the flux surface $v_{gr} = \frac{\partial\omega(k_y)}{\partial k_y}$ is compared to the phase velocity in the same direction $v_{ph} = \frac{\omega(k_y)}{k_y}$. Visually, $v_{ph} \approx v_{gr}$ for an intermediate scale $k_y\rho_s$ from 2 to 5, implying that waves in that range are weakly dispersive. The existence of this range can be understood from the fact that the ratio of the thermal banana orbit width to the ion sound gyroradius $\Delta r_b/\rho_s \approx 0.062$ is small, so there exists a range of scales where $k_y\rho_s$ is large enough that ions are largely adiabatic, while $k_y\Delta r_b$ is small enough that finite banana orbit width effects have yet to become important. Thus, TEMs at ion-scales are not expected to have this weak dispersion. Since the wave group velocity matches the phase velocity over a wide range in k, wave packets would travel with resonant particle trajectories in the absence of nonlinear scattering. As has been pointed out in the past,[59,60] since trapped electron bounce centers precess toroidally and do not decorrelate from the wave due to parallel streaming, they can remain at a fixed phase with the wave. This is contrasted with electrons and ions in passing orbits, which rapidly decorrelate with the wave phase due to parallel streaming. This long field-particle interaction time could lead to a large deflection of the trapped electron bounce center from its unperturbed trajectory. Such large deflections would lead to the breakdown of quasilinear theory, which is based on "small" kicks due to the response of particles to the perturbing fields.

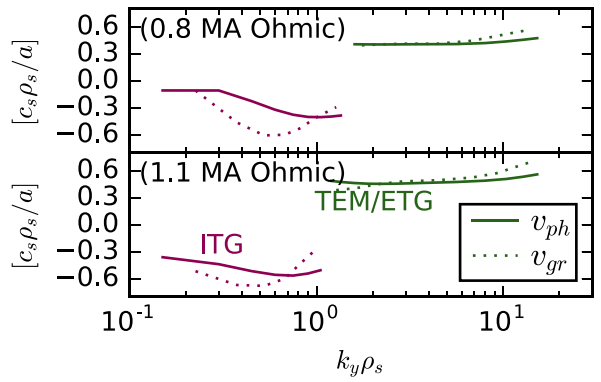

FIG. 8. A plot of wave phase velocity v_{ph} (solid lines) and group velocity v_{gr} (dashed lines), for both case I (top) and II (bottom) at $r/a = 0.6$. The ITG branch (magenta) and TEM/ETG branch (green) are shown in different colors. Note that v_{gr} follows v_{ph} more closely for the TEM/ETG branch than it does for the ITG branch. The text discusses this more quantitatively.

This breakdown is signaled quantitatively by the Kubo number $\mathcal{K} \equiv \tau_{ac}/\tau_S$ crossing unity. Here, τ_{ac} is the autocorrelation time of the fields (in this case, electrostatic potential) as seen by resonant particles on unperturbed trajectories, and τ_S is the "bounce" time of the resonant particle in the field pattern, after which the usage of unperturbed trajectories for resonant particles will fail. Some prototypical examples of τ_S are in Current Driven Ion Acoustic (CDIA) turbulence, where $\tau_S = \sqrt{q\tilde{\phi}/m_i}$ is the bounce time of a particle in an electrostatic well of amplitude $\tilde{\phi}$ formed by the ion acoustic wave or in fluid $E\times B$ turbulence, where $\tau_S = \tilde{V}_E/\lambda_c$ is the eddy circulation time with λ_c as the characteristic eddy length.[61] Here, the symbol τ_S is used to prevent confusion with the bounce time of particles in banana orbits τ_b in the magnetic well and emphasizes that this is an effect due to the long interaction time between particles and an eikonal phase S of the wave.

With this physical picture in mind, the proximity of v_{gr} to v_{ph} can now be estimated. Note that these are order of magnitude estimates, as the experiments do not tightly constrain many of the relevant values, and are presented here to inform future work rather than to claim any particular conclusion. For ITG, there are contributions from both parallel streaming and perpendicular particle drift motion relative to the group velocity, which we can estimate a typical time as $\tau_{ac,\parallel} \approx qR/v_{ti} \approx 5.4a/c_s$ and $\tau_{ac,\perp} \approx |(v_{ph}-v_{gr})\Delta k_y|^{-1} \approx 5a/c_s$, where $\Delta k_y\rho_s \approx 1$ for ITG and the phase and group velocity of the most unstable mode were taken. Thus, $\tau_{ac} = (\tau_{ac,\parallel}^{-1} + \tau_{ac,\perp}^{-1})^{-1} \approx 2.6a/c_s$. For the ITGb family, by using the values from Fig. 6 in Eq. (2), the experiment into heat flux requires a saturation amplitude of $\langle|\frac{e\tilde{\phi}}{T_e}|^2\rangle\frac{a^2}{\rho_s^2} \approx 1$ in the rotation reversal region. Using $T_e \approx 1.2T_i$ and considering a peak $k_y\rho_s \approx 0.5$, this amplitude corresponds to a typical RMS velocity of $\tilde{V}_E \approx 0.4c_s\rho_s/a$. Then, for radial eddies of size 2–10 ρ_s, the ITG Kubo number will be $\mathcal{K} \approx 0.5$–0.1, which marginally satisfies the requirements for quasilinear theory to hold. In contrast to this situation, for TEMs in the absence of collisions, the decorrelation will be due to the relative difference of the bounce center toroidal precession and the group velocity and can be estimated as $\tau_{ac} \approx |(v_{ph}-v_{gr})\Delta k_y|^{-1} \approx 25a/c_s$, where the spectral width $\Delta k_y\rho_s$ is taken to be 4, which is the spectral range over which the phase velocity closely follows the group velocity. For the TEMb family, a mixing length estimate constrained by the experimental fluxes suggests a saturation amplitude of $\langle|\frac{e\tilde{\phi}}{T_e}|^2\rangle\frac{a^2}{\rho_s^2} \approx 0.1$ in the rotation reversal region, so $\mathcal{K} \gtrsim 1$. Thus, the TEMb family does not satisfy a necessary condition for weak turbulence in LOC, when it is active.

As the transition is approached, the TEM amplitude decreases, lengthening τ_S. Concurrently, the collisionality increases, causing trapped electrons to be scattered into passing orbits, rapidly shortening τ_{ac}. These two effects suggest that $\mathcal{K}$ decreases as the LOC/SOC transition is approached, suggesting that the possibility of a transition from strong TEM turbulence to weak TEM turbulence may be involved with the transition. This transition could involve trapped electron coherent phase space structures in LOC, which disappear in SOC due to the stronger decorrelation mechanisms. These structures may take the form of coherent radial streamers, which have been observed in

simulations of strong collisionless TEM turbulence.[59] However, note that $\mathcal{K} < 1$ is necessary but not a sufficient condition for weak turbulence to hold, and other timescales such as the Dupree trapping time[62] or orbit dispersion from radial shear[63] need to be considered in order to determine if this strong to weak transition would actually occur.

An interesting meso-scale transition that could be involved in LOC/SOC is the formation of staircases. Staircases are self-sharpening zonal $E \times B$ flow patterns, named after their planetary analog.[64] The possibility of staircases being involved in LOC/SOC was raised by observations in Hornung *et al.*,[65] where quasi-regularly spaced local reductions in the radial turbulence coherence length were observed in SOC but not in LOC. Staircases could form from inhomogeneous mixing exhibiting bistability in the flux-gradient relationship. Staircase steps can merge to form larger shear layers.[66] The suggestion here would be that the fate of staircases would differ between LOC and SOC, possibly due to the stronger presence of TEM in the former. In LOC, staircases would either not form or not merge into large-scale shear layers, while in SOC, staircases would form and merge into the observed shear layer. One mechanism that could lead to this situation is the self-interaction of turbulent modes in the presence of trapped electrons, which have been observed in nonlinear gyrokinetic simulations to lead to the formation of small-scale shear structures that arrest the development of $E \times B$ staircases.[67] Another mechanism that could lead to this situation is suggested by the strong to weak turbulence transition mentioned earlier. In LOC, coherent trapped electron phase space structures could form and act as potential vorticity (PV) anomalies. Such PV anomalies would correspond to coherent vortices in atmospheric flows, which are known to punch through planetary staircases when the PV anomaly is large enough compared to the staircase PV step.[68]

VI. SUMMARY AND FUTURE WORK

In summary, this paper presents hysteresis experiments that provide a novel probe of the LOC/SOC transition and rotation reversal. The two transitions are shown to be linked to a single bifurcation of the turbulent state, showing that LOC and SOC correspond to different states of turbulence, with elements of this bifurcation persisting in auxiliary heated plasmas. Plasmas with density and temperature profiles indistinguishable within error bars are shown to manifest different rotation states, placing tight constraints on possible mechanisms for the rotation reversal. The hysteresis is observed to be robust to perturbative cold pulse injection, showing conclusively that a change in dominant ion-scale instability from electron-directed to ion-directed alone cannot be responsible for the LOC/SOC transition. Despite having nearly identical drive terms, differences in measured turbulent fluctuations are observed in some circumstances across the transition. Similar phenomena are observed in auxiliary heated L-modes, suggesting the relevance of the bifurcation to more general transport trends in L-mode. A reduced quasilinear transport model used experimentally inferred turbulent fluxes to provide constraints on the possible modes active in the turbulence. This analysis identified a change in the mix of mode saturation levels as a candidate explanation for the rotation reversal, implicating a subdominant mode population collapse as the physical mechanism underlying the observed bifurcation in turbulent fluctuations and momentum transport. This associates the LOC/SOC transition with the collapse of a subdominant intermediate-scale TEM population, rather than with a change in dominant linear instability from TEM to ITG. The relevance of physics beyond the quasilinear approximation was also explored, noting the possibility of a change from strong to weak TEM turbulence suggested by changes in the Kubo number across the transition.

The hysteresis experiments presented here provide a stepping stone for future inquiry that could lead to a full dynamical explanation of the LOC/SOC transition and rotation reversal. Many open questions remain since the validity of the quasilinear approximations is called into question in this work, and the mechanism underlying bistability has yet to be identified. Additionally, the link between how changes in turbulence lead to the observed changes in residual stress is still missing. The analysis hints at the nonlinear physics needed to construct reduced dynamical models to describe the LOC/SOC transition, such as predator-prey models of the sort used to describe the L–H transition. The experiments also suggest the possibility of numerical hysteresis experiments in global nonlinear simulations, which could probe the residual stress physics independent of the linear drives. The analysis also provides possible observable consequences of the bifurcation, which could be seen on present-day devices, providing interesting future experimental avenues of investigation as well.

ACKNOWLEDGMENTS

We thank Nathan T. Howard and Francesco Sciortino for their helpful advice on this work and also fruitful discussions at the 2018 Chengdu Theory Festival and 2019 Festival de Théorie. We also acknowledge the support of the Alcator C-Mod team, including the physics, engineering, and other technical staff. This work was supported by the U.S. Department of Energy, Office of Science, Office of Fusion Energy Sciences, under Award Nos. DE-FG02-04ER54738, DE-SC0014264, and DE-FC02-99ER54512.

REFERENCES

[1]P. Yushmanov, T. Takizuka, K. Riedel, O. Kardaun, J. Cordey, S. Kaye, and D. Post, "Scalings for tokamak energy confinement," Nucl. Fusion **30**, 1999–2006 (1990).
[2]ITER Physics Expert Group on Confin Transport, ITER Physics Expert Group on Confin Database, and ITER Physics Basis Editors, "Chapter 2: Plasma confinement and transport," Nucl. Fusion **39**, 2175–2249 (1999).
[3]F. Wagner and U. Stroth, "Transport in toroidal devices-the experimentalist's view," Plasma Phys. Controlled Fusion **35**, 1321–1371 (1993).
[4]J. Rice, C. Gao, M. Reinke, P. Diamond, N. Howard, H. Sun, I. Cziegler, A. Hubbard, Y. Podpaly, W. Rowan, J. Terry, M. Chilenski, L. Delgado-Aparicio, P. Ennever, D. Ernst, M. Greenwald, J. Hughes, Y. Ma, E. Marmar, M. Porkolab, A. White, and S. Wolfe, "Non-local heat transport, rotation reversals and up/down impurity density asymmetries in Alcator C-Mod ohmic L-mode plasmas," Nucl. Fusion **53**, 033004 (2013).
[5]H. Arnichand, R. Sabot, S. Hacquin, A. Krämer-Flecken, X. Garbet, J. Citrin, C. Bourdelle, G. Hornung, J. Bernardo, C. Bottereau, F. Clairet, G. Falchetto, and J. Giacalone, "Quasi-coherent modes and electron-driven turbulence," Nucl. Fusion **54**, 123017 (2014).
[6]Y. Shi, J. Kwon, P. Diamond, W. Ko, M. Choi, S. Ko, S. Hahn, D. Na, J. Leem, J. Lee, S. Yang, K. Lee, M. Joung, J. Jeong, J. Yoo, W. Lee, J. Lee, Y. Bae, S. Lee, S. Yoon, K. Ida, and Y.-S. Na, "Intrinsic rotation reversal, non-local transport, and turbulence transition in KSTAR L-mode plasmas," Nucl. Fusion **57**, 066040 (2017).
[7]F. Romanelli, W. Tang, and R. White, "Anomalous thermal confinement in ohmically heated tokamaks," Nucl. Fusion **26**, 1515–1528 (1986).
[8]I. Erofeev, E. Fable, C. Angioni, and R. McDermott, "Theory-based modeling of LOC-SOC transitions in ASDEX Upgrade," Nucl. Fusion **57**, 126067 (2017).

[9]B. A. Grierson, C. Chrystal, S. R. Haskey, W. X. Wang, T. L. Rhodes, G. R. McKee, K. Barada, X. Yuan, M. F. F. Nave, A. Ashourvan, and C. Holland, "Main-ion intrinsic toroidal rotation across the ITG/TEM boundary in DIII-D discharges during ohmic and electron cyclotron heating," Phys. Plasmas **26**, 042304 (2019).
[10]J. E. Rice, I. Cziegler, P. H. Diamond, B. P. Duval, Y. A. Podpaly, M. L. Reinke, P. C. Ennever, M. J. Greenwald, J. W. Hughes, Y. Ma, E. S. Marmar, M. Porkolab, N. Tsujii, and S. M. Wolfe, "Rotation reversal bifurcation and energy confinement saturation in tokamak ohmic L-mode plasmas," Phys. Rev. Lett. **107**, 265001 (2011).
[11]J. Rice, B. Duval, M. Reinke, Y. Podpaly, A. Bortolon, R. Churchill, I. Cziegler, P. Diamond, A. Dominguez, P. Ennever, C. Fiore, R. Granetz, M. Greenwald, A. Hubbard, J. Hughes, J. Irby, Y. Ma, E. Marmar, R. McDermott, M. Porkolab, N. Tsujii, and S. Wolfe, "Observations of core toroidal rotation reversals in Alcator C-Mod ohmic L-mode plasmas," Nucl. Fusion **51**, 083005 (2011).
[12]C. Sung, A. White, N. Howard, C. Oi, J. Rice, C. Gao, P. Ennever, M. Porkolab, F. Parra, D. Mikkelsen, D. Ernst, J. Walk, J. Hughes, J. Irby, C. Kasten, A. Hubbard, and M. Greenwald, "Changes in core electron temperature fluctuations across the ohmic energy confinement transition in Alcator C-Mod plasmas," Nucl. Fusion **53**, 083010 (2013).
[13]C. Sung, A. E. White, D. R. Mikkelsen, M. Greenwald, C. Holland, N. T. Howard, R. Churchill, and C. Theiler, "Quantitative comparison of electron temperature fluctuations to nonlinear gyrokinetic simulations in C-Mod ohmic L-mode discharges," Phys. Plasmas **23**, 042303 (2016).
[14]R. McDermott, C. Angioni, G. Conway, R. Dux, E. Fable, R. Fischer, T. Pütterich, F. Ryter, and E. Viezzer, "Core intrinsic rotation behaviour in ASDEX Upgrade ohmic L-mode plasmas," Nucl. Fusion **54**, 043009 (2014).
[15]N. Cao, J. Rice, P. Diamond, A. White, S. Baek, M. Chilenski, J. Hughes, J. Irby, M. Reinke, and P. Rodriguez-Fernandez, "Hysteresis as a probe of turbulent bifurcation in intrinsic rotation reversals on Alcator C-Mod," Nucl. Fusion **59**, 104001 (2019).
[16]A. Bortolon, B. P. Duval, A. Pochelon, and A. Scarabosio, "Observation of spontaneous toroidal rotation inversion in ohmically heated tokamak plasmas," Phys. Rev. Lett. **97**, 235003 (2006).
[17]P. Rodriguez-Fernandez, A. E. White, N. T. Howard, B. A. Grierson, G. M. Staebler, J. E. Rice, X. Yuan, N. M. Cao, A. J. Creely, M. J. Greenwald, A. E. Hubbard, J. W. Hughes, J. H. Irby, and F. Sciortino, "Explaining cold-pulse dynamics in tokamak plasmas using local turbulent transport models," Phys. Rev. Lett. **120**, 075001 (2018).
[18]P. Rodriguez-Fernandez, A. White, N. Howard, B. Grierson, X. Yuan, G. Staebler, J. Rice, C. Angioni, N. Cao, A. Creely, E. Fable, M. Greenwald, A. Hubbard, J. Hughes, J. Irby, and F. Sciortino, "Perturbative transport modeling of cold-pulse dynamics in Alcator C-Mod ohmic plasmas," Nucl. Fusion **59**, 066017 (2019).
[19]T. Ohkawa, "A transport model for alcator scaling in tokamaks," Phys. Lett. A **67**, 35–38 (1978).
[20]A. G. Peeters and C. Angioni, "Linear gyrokinetic calculations of toroidal momentum transport in a tokamak due to the ion temperature gradient mode," Phys. Plasmas **12**, 072515 (2005).
[21]P. H. Diamond, C. J. McDevitt, Ö. D. Gürcan, T. S. Hahm, and V. Naulin, "Transport of parallel momentum by collisionless drift wave turbulence," Phys. Plasmas **15**, 012303 (2008).
[22]L. Wang and P. H. Diamond, "Gyrokinetic theory of turbulent acceleration of parallel rotation in tokamak plasmas," Phys. Rev. Lett. **110**, 265006 (2013).
[23]A. Peeters, C. Angioni, A. Bortolon, Y. Camenen, F. Casson, B. Duval, L. Fiederspiel, W. Hornsby, Y. Idomura, T. Hein, N. Kluy, P. Mantica, F. Parra, A. Snodin, G. Szepesi, D. Strintzi, T. Tala, G. Tardini, P. de Vries, and J. Weiland, "Overview of toroidal momentum transport," Nucl. Fusion **51**, 094027 (2011).
[24]P. Diamond, Y. Kosuga, Ö. Gürcan, C. McDevitt, T. Hahm, N. Fedorczak, J. Rice, W. Wang, S. Ku, J. Kwon, G. Dif-Pradalier, J. Abiteboul, L. Wang, W. Ko, Y. Shi, K. Ida, W. Solomon, H. Jhang, S. Kim, S. Yi, S. Ko, Y. Sarazin, R. Singh, and C. Chang, "An overview of intrinsic torque and momentum transport bifurcations in toroidal plasmas," Nucl. Fusion **53**, 104019 (2013).
[25]Y. Camenen, C. Angioni, A. Bortolon, B. P. Duval, E. Fable, W. A. Hornsby, R. M. McDermott, D. H. Na, Y.-S. Na, A. G. Peeters, and J. E. Rice, "Experimental observations and modelling of intrinsic rotation reversals in tokamaks," Plasma Phys. Controlled Fusion **59**, 034001 (2017).
[26]W. X. Wang, P. H. Diamond, T. S. Hahm, S. Ethier, G. Rewoldt, and W. M. Tang, "Nonlinear flow generation by electrostatic turbulence in tokamaks," Phys. Plasmas **17**, 072511 (2010).
[27]J. Kwon, S. Yi, T. Rhee, P. Diamond, K. Miki, T. Hahm, J. Kim, Ö. Gürcan, and C. McDevitt, "Analysis of symmetry breaking mechanisms and the role of turbulence self-regulation in intrinsic rotation," Nucl. Fusion **52**, 013004 (2012).
[28]B. A. Grierson, W. X. Wang, S. Ethier, G. M. Staebler, D. J. Battaglia, J. A. Boedo, J. S. DeGrassie, and W. M. Solomon, "Main-ion intrinsic toroidal rotation profile driven by residual stress torque from ion temperature gradient turbulence in the DIII-D tokamak," Phys. Rev. Lett. **118**, 015002 (2017).
[29]W. A. Hornsby, C. Angioni, Z. X. Lu, E. Fable, I. Erofeev, R. McDermott, A. Medvedeva, A. Lebschy, and A. G. Peeters, "Global gyrokinetic simulations of intrinsic rotation in ASDEX Upgrade ohmic L-mode plasmas," Nucl. Fusion **58**, 056008 (2018).
[30]H. Arnichand, J. Citrin, S. Hacquin, R. Sabot, A. Krämer-Flecken, X. Garbet, C. Bourdelle, C. Bottereau, F. Clairet, J. C. Giacalone, Z. O. Guimarães-Filho, R. Guirlet, G. Hornung, A. Lebschy, P. Lotte, P. Maget, A. Medvedeva, D. Molina, V. Nikolaeva, and D. Prisiazhniuk, "Identification of trapped electron modes in frequency fluctuation spectra," Plasma Phys. Controlled Fusion **58**, 014037 (2016).
[31]J. Citrin, H. Arnichand, J. Bernardo, C. Bourdelle, X. Garbet, F. Jenko, S. Hacquin, M. J. Pueschel, and R. Sabot, "Comparison between measured and predicted turbulence frequency spectra in ITG and TEM regimes," Plasma Phys. Controlled Fusion **59**, 064010 (2017).
[32]M. Greenwald, A. Bader, S. Baek, M. Bakhtiari, H. Barnard, W. Beck, W. Bergerson, I. Bespamyatnov, P. Bonoli, D. Brower, D. Brunner, W. Burke, J. Candy, M. Churchill, I. Cziegler, A. Diallo, A. Dominguez, B. Duval, E. Edlund, P. Ennever, D. Ernst, I. Faust, C. Fiore, T. Fredian, O. Garcia, C. Gao, J. Goetz, T. Golfinopoulos, R. Granetz, O. Grulke, Z. Hartwig, S. Horne, N. Howard, A. Hubbard, J. Hughes, I. Hutchinson, J. Irby, V. Izzo, C. Kessel, B. LaBombard, C. Lau, C. Li, Y. Lin, B. Lipschultz, A. Loarte, E. Marmar, A. Mazurenko, G. McCracken, R. McDermott, O. Meneghini, D. Mikkelsen, D. Mossessian, R. Mumgaard, J. Myra, E. Nelson-Melby, R. Ochoukov, G. Olynyk, R. Parker, S. Pitcher, Y. Podpaly, M. Porkolab, M. Reinke, J. Rice, W. Rowan, A. Schmidt, S. Scott, S. Shiraiwa, J. Sierchio, N. Smick, J. A. Snipes, P. Snyder, B. Sorbom, J. Stillerman, C. Sung, Y. Takase, V. Tang, J. Terry, D. Terry, C. Theiler, A. Tronchin-James, N. Tsujii, R. Vieira, J. Walk, G. Wallace, A. White, D. Whyte, J. Wilson, S. Wolfe, G. Wright, J. Wright, S. Wukitch, and S. Zweben, "20 years of research on the alcator C-Mod tokamak," Phys. Plasmas **21**, 110501 (2014).
[33]N. M. Cao and F. Sciortino, "Bayesian spectral moment estimation and uncertainty quantification," IEEE Trans. Plasma Sci. **48**, 22–29 (2020).
[34]M. Chilenski, M. Greenwald, Y. Marzouk, N. Howard, A. White, J. Rice, and J. Walk, "Improved profile fitting and quantification of uncertainty in experimental measurements of impurity transport coefficients using Gaussian process regression," Nucl. Fusion **55**, 023012 (2015).
[35]J. E. Rice, M. J. Greenwald, Y. A. Podpaly, M. L. Reinke, P. H. Diamond, J. W. Hughes, N. T. Howard, Y. Ma, I. Cziegler, B. P. Duval, P. C. Ennever, D. Ernst, C. L. Fiore, C. Gao, J. H. Irby, E. S. Marmar, M. Porkolab, N. Tsujii, and S. M. Wolfe, "Ohmic energy confinement saturation and core toroidal rotation reversal in Alcator C-Mod plasmas," Phys. Plasmas **19**, 056106 (2012).
[36]M. L. Reinke, J. E. Rice, A. E. White, M. Greenwald, N. T. Howard, P. Ennever, C. Gao, A. E. Hubbard, and J. W. Hughes, "Density sensitivity of intrinsic rotation profiles in ion cyclotron range of frequency-heated L-mode plasmas," Plasma Phys. Controlled Fusion **55**, 012001 (2013).
[37]M. Porkolab, J. Rost, N. Basse, J. Dorris, E. Edlund, L. Lin, Y. Lin, and S. Wukitch, "Phase contrast imaging of waves and instabilities in high temperature magnetized fusion plasmas," IEEE Trans. Plasma Sci. **34**, 229–234 (2006).
[38]P. Ennever, "Turbulence and transport measurements in Alcator C-Mod and comparisons with gyrokinetic simulations," Ph.D. thesis (Massachusetts Institute of Technology, 2016).
[39]J. Candy, E. Belli, and R. Bravenec, "A high-accuracy Eulerian gyrokinetic solver for collisional plasmas," J. Comput. Phys. **324**, 73–93 (2016).
[40]R. E. Waltz, A. Casati, and G. M. Staebler, "Gyrokinetic simulation tests of quasilinear and tracer transport," Phys. Plasmas **16**, 072303 (2009).

[41]A. E. White, W. A. Peebles, T. L. Rhodes, C. H. Holland, G. Wang, L. Schmitz, T. A. Carter, J. C. Hillesheim, E. J. Doyle, L. Zeng, G. R. McKee, G. M. Staebler, R. E. Waltz, J. C. DeBoo, C. C. Petty, and K. H. Burrell, "Measurements of the cross-phase angle between density and electron temperature fluctuations and comparison with gyrokinetic simulations," Phys. Plasmas **17**, 056103 (2010).
[42]S. J. Freethy, T. Görler, A. J. Creely, G. D. Conway, S. S. Denk, T. Happel, C. Koenen, P. Hennequin, and A. E. White, "Validation of gyrokinetic simulations with measurements of electron temperature fluctuations and density-temperature phase angles on ASDEX Upgrade," Phys. Plasmas **25**, 055903 (2018).
[43]G. M. Staebler, J. E. Kinsey, and R. E. Waltz, "A theory-based transport model with comprehensive physics," Phys. Plasmas **14**, 055909 (2007).
[44]C. Bourdelle, X. Garbet, F. Imbeaux, A. Casati, N. Dubuit, R. Guirlet, and T. Parisot, "A new gyrokinetic quasilinear transport model applied to particle transport in tokamak plasmas," Phys. Plasmas **14**, 112501 (2007).
[45]J. Breslau, M. Gorelenkova, F. Poli, J. Sachdev, X. Yuan, and USDOE Office of Science, TRANSP. Computer software, USDOE Office of Science (SC), Fusion Energy Sciences (FES) (SC-24), 2018, available at https://www.osti.gov/biblio/1489900-transp.
[46]E. A. Belli and J. Candy, "Kinetic calculation of neoclassical transport including self-consistent electron and impurity dynamics," Plasma Phys. Controlled Fusion **50**, 095010 (2008).
[47]C. Angioni, Y. Camenen, F. Casson, E. Fable, R. McDermott, A. Peeters, and J. Rice, "Off-diagonal particle and toroidal momentum transport: A survey of experimental, theoretical and modelling aspects," Nucl. Fusion **52**, 114003 (2012).
[48]B. Coppi and F. Pegoraro, "Theory of the ubiquitous mode," Nucl. Fusion **17**, 969–993 (1977).
[49]F. I. Parra and P. J. Catto, "Vorticity and intrinsic ambipolarity in turbulent tokamaks," Plasma Phys. Controlled Fusion **51**, 095008 (2009).
[50]R. E. Waltz, R. L. Dewar, and X. Garbet, "Theory and simulation of rotational shear stabilization of turbulence," Phys. Plasmas **5**, 1784–1792 (1998).
[51]Y. Camenen, Y. Idomura, S. Jolliet, and A. Peeters, "Consequences of profile shearing on toroidal momentum transport," Nucl. Fusion **51**, 073039 (2011).
[52]P. H. Diamond, Y.-M. Liang, B. A. Carreras, and P. W. Terry, "Self-regulating shear flow turbulence: A paradigm for the L to H transition," Phys. Rev. Lett. **72**, 2565–2568 (1994).
[53]H. Biglari, P. H. Diamond, and P. W. Terry, "Influence of sheared poloidal rotation on edge turbulence," Phys. Fluids B **2**, 1–4 (1990).
[54]T. S. Hahm and K. H. Burrell, "Flow shear induced fluctuation suppression in finite aspect ratio shaped tokamak plasma," Phys. Plasmas **2**, 1648–1651 (1995).
[55]J. Lang, Y. Chen, and S. E. Parker, "Gyrokinetic δf particle simulation of trapped electron mode driven turbulence," Phys. Plasmas **14**, 082315 (2007).
[56]F. Merz and F. Jenko, "Nonlinear saturation of trapped electron modes via perpendicular particle diffusion," Phys. Rev. Lett. **100**, 035005 (2008).
[57]J. Lang, S. E. Parker, and Y. Chen, "Nonlinear saturation of collisionless trapped electron mode turbulence: Zonal flows and zonal density," Phys. Plasmas **15**, 055907 (2008).
[58]D. R. Ernst, J. Lang, W. M. Nevins, M. Hoffman, Y. Chen, W. Dorland, and S. Parker, "Role of zonal flows in trapped electron mode turbulence through nonlinear gyrokinetic particle and continuum simulation," Phys. Plasmas **16**, 055906 (2009).
[59]Y. Xiao and Z. Lin, "Turbulent transport of trapped-electron modes in collisionless plasmas," Phys. Rev. Lett. **103**, 085004 (2009).
[60]Y. Kosuga, S.-I. Itoh, P. H. Diamond, K. Itoh, and M. Lesur, "Ion temperature gradient driven turbulence with strong trapped ion resonance," Phys. Plasmas **21**, 102303 (2014).
[61]R. Z. Sagdeev and A. A. Galeev, *Nonlinear Plasma Theory* (Benjamin, New York, 1969).
[62]T. H. Dupree, "A perturbation theory for strong plasma turbulence," Phys. Fluids **9**, 1773 (1966).
[63]G. J. Choi and T. S. Hahm, "E×B shear and precession shear induced turbulence suppression and its influence on electron thermal internal transport barrier formation," Phys. Plasmas **23**, 072301 (2016).
[64]G. Dif-Pradalier, P. H. Diamond, V. Grandgirard, Y. Sarazin, J. Abiteboul, X. Garbet, P. Ghendrih, A. Strugarek, S. Ku, and C. S. Chang, "On the validity of the local diffusive paradigm in turbulent plasma transport," Phys. Rev. E **82**, 025401 (2010).
[65]G. Hornung, G. Dif-Pradalier, F. Clairet, Y. Sarazin, R. Sabot, P. Hennequin, and G. Verdoolaege, "$\mathbf{E} \times \mathbf{B}$ Staircases and barrier permeability in magnetised plasmas," Nucl. Fusion **57**, 014006 (2017).
[66]A. Ashourvan and P. H. Diamond, "How mesoscopic staircases condense to macroscopic barriers in confined plasma turbulence," Phys. Rev. E **94**, 051202 (2016).
[67]A. Weikl, A. G. Peeters, F. Rath, F. Seiferling, R. Buchholz, S. R. Grosshauser, and D. Strintzi, "The occurrence of staircases in ITG turbulence with kinetic electrons and the zonal flow drive through self-interaction," Phys. Plasmas **25**, 072305 (2018).
[68]D. G. Dritschel and M. E. McIntyre, "Multiple jets as PV staircases: The Phillips effect and the resilience of Eddy-transport barriers," J. Atmos. Sci. **65**, 855–874 (2008).